Geochemical Perspectives Letters

Intramolecular fractionation of hydrogen isotopes in silicate quenched melts

C. Le Losq[1,2*], B.O. Mysen[1], G.D. Cody[1]

OPEN ACCESS

doi: 10.7185/geochemlet.1609

Abstract

The interplay between the chemical composition and the molecular structure of silicate melts was central to the evolution of the Earth's crust, mantle and core. This interplay also affects geochemical records such as the partitioning of isotopes between minerals, melts and fluids in the Earth's interior. For instance, large $^{2}H/^{1}H$ fractionations between silicate melts and aqueous fluids have been observed at high temperature and pressure. Such behaviour may be promoted by the occurrence of $^{2}H/^{1}H$ intramolecular fractionation within the molecular structure of silicate melts. New Raman spectroscopy and ^{1}H and ^{2}H Nuclear Magnetic Resonance (NMR) spectroscopy data reveal the source of such $^{2}H/^{1}H$ intramolecular isotopic fractionation, showing that ^{1}H and ^{2}H fractionate between the silicate tetrahedral units. Such a process might affect other isotopic systems (*e.g.*, N, C, or S) where the isotopes interact with the melt silicate network.

Received 24 November 2015 | Accepted 21 January 2016 | Published 16 February 2016

Introduction

Silicate melts played a determining role in the segregation and evolution of the Earth's crust, mantle and core (*e.g.*, Wood *et al.*, 2006; Labrosse *et al.*, 2007). Characterisation of their structure is central to understanding those processes. The silicate melt structure comprises *network forming* ions (Si^{4+}, Al^{3+}, Fe^{3+}…) in interconnected oxygen polyhedra, forming a network that can be disrupted by *network modifiers* ions, *e.g.*, Mg^{2+}, Ca^{2+}, K^{+}, Na^{+}. The latter may also act as *charge compensators* of the O^{2-} bonded to *network forming* trivalent cations. Additional complexity arises from large variations in Si-O-Si / Si-O-Al bond angles and cationic coordination numbers, and non-random mixing and partitioning of the cations (Mysen and Richet, 2005; Greaves and Sen, 2007).

1. Geophysical Laboratory, Carnegie Institution of Washington, 5251 Broad Branch Road NW, 20015 Washington D.C., USA
2. Present address: Research School of Earth Sciences, The Australian National University, Building 142, Mills Road, ACT 2601 Canberra, Australia
* Corresponding author (email: charles.lelosq@anu.edu.au)

From this structural complexity may arise peculiar effects on the partitioning of isotopes between silicate melts, minerals, and aqueous fluids. For example, the partitioning of $^{15}N/^{14}N$, of $^{13}C/^{12}C$, and of $^{2}H/^{1}H$ between sodium silicate melts and aqueous fluids depends on the melt structure (Mysen *et al.*, 2009; Mysen and Fogel, 2010). The $^{34}S/^{32}S$ fractionation between aluminosilicate melts and metals also depends on the proportion of *network formers* Al^{3+} or B^{3+} in the melts (Labidi *et al.*, 2016). Further, the behaviour of Fe isotopes in silicate melts is affected by the effects of melt composition on the Fe environment (Dauphas *et al.*, 2014).

The ^{2}H and ^{1}H isotopes may be particularly strongly affected by intramolecular processes in silicate melts because of their large difference in mass. Results from ^{1}H and ^{2}H Rotor-synchronised Magic-Angle Spinning (MAS) Nuclear Magnetic Resonance (NMR) spectroscopy of hydrous sodium tetrasilicate and MORB-like glasses indicate that ^{2}H tends to populate environments with shorter O-O distances compared to ^{1}H in quenched melts (Wang *et al.*, 2015). Therefore, ^{2}H and ^{1}H seem to fractionate between the various molecular environments in silicate melts.

Such $^{2}H/^{1}H$ intramolecular fractionation may help understanding the large $^{2}H/^{1}H$ isotopic fractionation observed between silicate melts and aqueous fluids. Indeed, *in situ* Raman observations in diamond cells show that $\alpha_{fluid\text{-}melt} = \left(\frac{^{2}H}{^{1}H}\right)_{fluid} / \left(\frac{^{2}H}{^{1}H}\right)_{melt}$ may reach hundreds of ‰ at temperatures and pressures as high as 700 °C and 1.5 GPa (Mysen, 2013a,b; Dalou *et al.*, 2015). Such values are higher than typical $\alpha_{fluid\text{-}mineral}$ in the tens of ‰ level (Chacko *et al.*, 2001). According to the results of Wang *et al.* (2015), the intramolecular fractionation of ^{2}H and ^{1}H in silicate melts results in differences between the mean O-^{1}H and O-^{2}H bond lengths. Therefore, it may enhance the differences of O-^{1}H and O-^{2}H bond strengths between silicate melts and aqueous fluids, and, as a result, promote a strong fractionation of both isotopes between those substances (Schauble, 2004 and references therein).

To gain further understanding of such process, we performed Raman spectroscopy and ^{1}H and ^{2}H Rotor-synchronised MAS NMR observations of $Li_2Si_4O_9$, $Na_2Si_4O_9$ and $K_2Si_4O_9$ melts quenched from high temperature and pressure, and containing $^{1}H_2O$, $^{2}H_2O$, or a mixture of both (Table S-1). Experimental methods are described in Supplementary Information and all acquired NMR and Raman spectra are provided in Supplementary Figures S-1, S-2, S-3 and S-4.

Results

^{1}H and ^{2}H isotropic NMR spectra of the hydrous alkali quenched melts present three main peaks near 16, 5 and 1.8 ppm in three frequency regions, HF, MF and LF (Fig. 1, Supplementary Information). The ^{2}H signal is systematically more intense in the HF region and less intense in the MF region relative to that

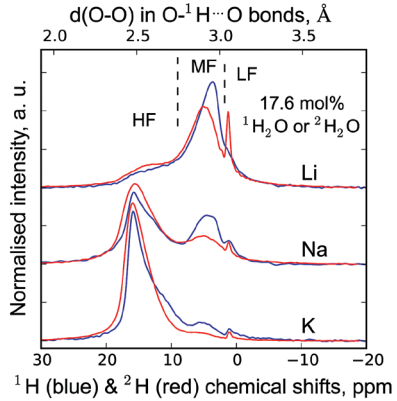

Figure 1 ^{1}H and ^{2}H isotropic MAS NMR spectra of the alkali tetrasilicate glasses containing 17.6 mol % of pure ^1H_2O or ^2H_2O. O-O distances along O-H···O bonds have been determined from the ^{1}H chemical shifts following Xue and Kanzaki (2009).

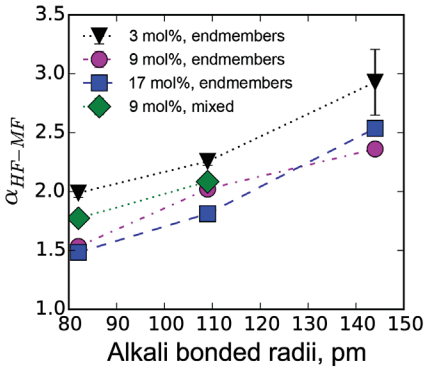

Figure 2 $\alpha_{HF\text{-}MF}$ (= $(^2H/^1H)_{HF}$ / $(^2H/^1H)_{MF}$) intramolecular fractionation factors between the environments linked to the HF and MF regions in the ^{1}H and ^{2}H NMR spectra (Supplementary Information). Inverted triangles, circles and squares: determined from the NMR data of *"endmembers"* glasses containing pure ^1H_2O and pure ^2H_2O; diamonds: determined from the NMR data of the glasses with mixed ^1H_2O-^2H_2O (1:1 ratio; no fractionation factor is provided at 144 pm as the NMR data for K-bearing glass were too noisy to provide an accurate estimation). Alkali bonded radii are from Gibbs *et al.* (2014), assuming 6 fold coordinated alkalis.

of ^{1}H at any water content and glass composition (Fig. 1). The intensity in the LF region of the ^{1}H and ^{2}H NMR spectra also differs, but in a non systematic way such that it is difficult to ascribe those changes to an isotopic effect. Furthermore, the area of the LF peak constitutes a small (<5 %) fraction of the total integrated NMR intensity. For those reasons, we will not consider it further.

The differences in ^{2}H and ^{1}H isotropic NMR spectra indicate that ^{2}H and ^{1}H fractionate between different environments in the silicate melt structure, with ^{2}H preferentially populating environments with small O-O distances (Fig. 1). This effect can be quantified by calculating the fractionation factor between the HF and MF spectral regions, $\alpha_{HF\text{-}MF}$ (Fig. 2). $\alpha_{HF\text{-}MF}$ depends primarily on the alkali ionic radius, as shown by a ~65 % variation between the Li and K glasses, and secondarily on the glass water content. The latter influence probably originates from the fact that increasing the water content increases the fraction of molecular water, which gives a weak signal in the MF portion of ^{2}H and ^{1}H NMR spectra.

The signals in the 850-1300 cm^{-1} portion of the Raman spectra of glasses with comparable composition and water content, but containing either pure ^1H_2O or pure ^2H_2O, systematically differ from each other (Fig. 3). The intensity of the signal assigned to Si-O stretching in Q^3 units (~1100 cm^{-1}) is enhanced by the presence of ^2H_2O, whereas that assigned to Si-O

stretching in Q^2 units (~950 cm^{-1}) is lowered (Supplementary Information for additional detail). This observation is confirmed by subtraction of the Raman spectra of the ^1H_2O-bearing glasses from those of the ^2H_2O-bearing glasses (Fig. 3b). The variations of the intensity near 1150-1200 cm^{-1}, where the signal from Si-O stretching in Q^4 units occurs, are negligible compared with those of the ~950 and ~1100 cm^{-1} signals.

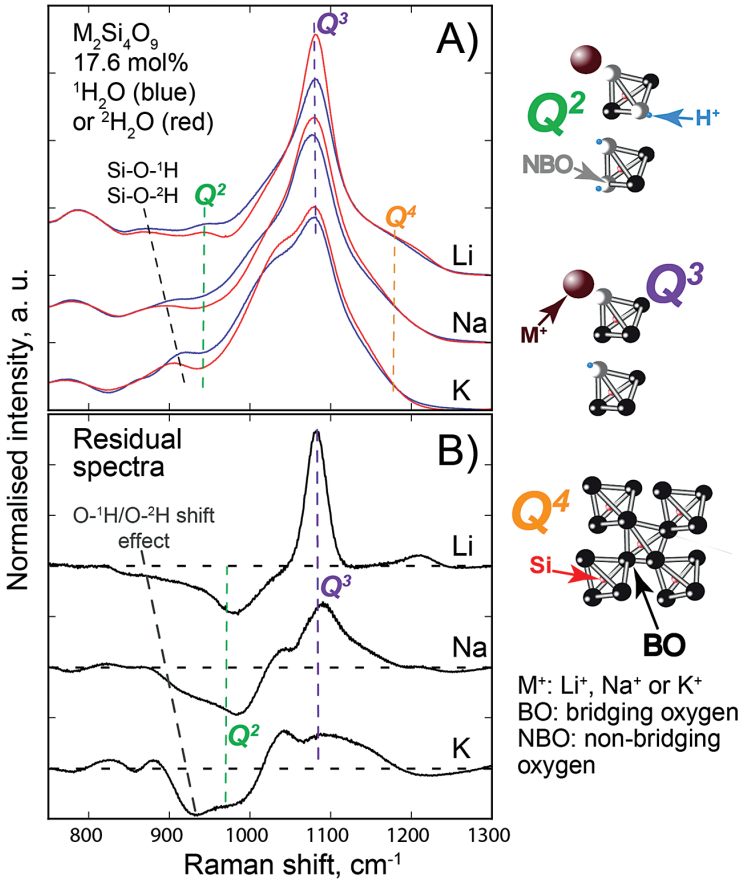

Figure 3 **(a)** 750-1300 cm^{-1} portion of Raman spectra of the alkali silicate glasses containing 17.6 mol % of pure ^1H_2O (blue lines) or ^2H_2O (red lines). **(b)** Residual spectra from the subtraction of the Raman spectra of the ^1H_2O-bearing glasses from those of the ^2H_2O-bearing glasses. The contributions between 850 and 930 cm^{-1} are artifacts resulting from the frequency shift of the Si-O-H stretching vibration upon ^{2}H/^{1}H substitution. On the right part of this figure are presented schemes of the Q^n SiO_4 tetrahedral units, containing *n* bridging and 4-*n* non-bridging oxygen atoms, that form the molecular disordered backbone of silicate melts.

Discussion

The decrease of the Q^2 abundance and the increase of the Q^3 abundance by substitution of ^1H for ^2H seen in the Raman spectra of the glasses explain the variations of the ^1H and ^2H NMR signals. Indeed, from $\{^1H\}$-^{29}Si HETCOR NMR data of $Na_2Si_4O_9$ hydrous glasses (Robert *et al.*, 2001), the ^1H 16 ppm NMR signal is strongly correlated with the ^{29}Si NMR signal from Q^3 units, and is only weakly correlated with that of Q^2 units. An increase of Q^3 abundance with substitution of ^1H by ^2H in the glasses thus explains the higher ^2H NMR signal near 16 ppm (Figs. 1, S-1, S-2). Therefore, we conclude that, compared to ^1H, ^2H preferentially bonds with non-bridging oxygens in Q^3 units relative to Q^2 units. From the variations in the Raman signal intensity, the differences range between 0.5 and 4 %.

This intramolecular fractionation of ^2H and ^1H between the Q^n units explains the variations of $\alpha_{HF\text{-}MF}$ as a function of composition (Fig. 2). Indeed, with increasing alkali ionic radius, both the distribution of Q^n species and the proton environment change (Le Losq *et al.*, 2015). These factors affect the $^2H/^1H$ intramolecular fractionation. The latter probably occurs at high temperature in the molten state, far from the melt glass transition temperature, *Tg*. This hypothesis is supported by the fact that the quench rate affects the *Tg* and the water speciation (*e.g.*, Behrens and Yamashita, 2008), but has no effect on the $^2H/^1H$ intramolecular fractionation (Wang *et al.*, 2015).

Wang *et al.* (2015) proposed that the intramolecular fractionation of ^1H and ^2H observed in the glasses arises from a molar volume isotope effect (*e.g.*, Driesner *et al.*, 1997), which may be analogous to that observed in the brucite-water system (Horita *et al.*, 1999, 2002, 2010). Following Wang *et al.* (2015), ^2H would preferentially occupy environments in silicate melts with smaller O-O distances, and hence volumes compared to ^1H, explaining the ^2H and ^1H NMR data (Fig. 1). The present Raman data offer further understanding by showing the bonding preferences of ^2H and ^1H for different silicate units in the glasses. Such bonding preferences may result from different "effective" ionic radii of ^1H and ^2H in silicate melts, induced by their different quantum mechanical properties. This is analogous to the alkali ionic radius effect on the Q^n units distribution in silicate melts (*e.g.*, Maekawa *et al.*, 1991).

The equilibrium fractionation of isotopes between different substances is governed by the different strengths of the bonds that the isotopes form in the substances (Schauble, 2004 and references therein). In silicate melts at high temperature, water is mostly present as OH groups (*e.g.*, Behrens and Yamashita, 2008), with protons interacting with the Q^n units. The present data indicate that, in such conditions, ^2H populates the environments characterised by short O-O distances, and, hence long O-H bonds, slightly more than does ^1H (Fig. 1, the shortening of O-O bonds around protons enhances hydrogen bonding, pulling away the protons from the "primary" O, see Novak, 1974). As a result, the mean O-^2H bond strength will be less than the mean O-^1H bond strength in the melt.

Such phenomena may affect the differences in O-^2H bond strength between silicate melts and aqueous fluids. Therefore, these structural features can control the isotopic fractionation of ^2H and ^1H between the melts and the fluids. This theory might explain the large fractionation of ^2H and ^1H between those substances (Mysen, 2013a,b; Dalou *et al.*, 2015).

The link between the chemical composition and the speciation of Q^n units (*e.g.*, Mysen and Richet, 2005) implies that the intramolecular fractionation of ^2H and ^1H depends on the melt composition (Fig. 2). This may result in compositionally-dependent $\alpha_{fluid\text{-}melt}$, $\alpha_{vapour\text{-}melt}$ and $\alpha_{mineral\text{-}melt}$ fractionation factors, correlated with magmatic differentiation. Moreover, the intramolecular fractionation effect affects the fraction of water that interacts structurally with the silicate network, *i.e.* the so-called hydroxyl groups. Therefore, the influence of this effect on the $\alpha_{fluid\text{-}melt}$, $\alpha_{vapour\text{-}melt}$ and $\alpha_{mineral\text{-}melt}$ fractionation factors can also depend on water speciation. This may not be crucial at high temperatures where most of the water resides as OH groups in the melt, but it might play a determining role at temperatures corresponding to superficial volcanism, where magma degassing occurs. Such an idea agrees with an $\alpha_{vapour\text{-}melt}$ that depends on water speciation (De Hoog *et al.*, 2009 and references therein).

The discussion above emphasises the centrally important principles that affect $^2H/^1H$ fractionation with implications for a range of geochemical problems. However, quantitative characterisation of how intramolecular fractionation of ^2H and ^1H in silicate melts governs hydrogen isotope fractionation processes in nature remain to be assessed. This fractionation of ^2H and ^1H between the Q^n units of silicate melts likely reflects different extents of steric hindrance. This is analogous to the different distribution of alkali metals among structural units, for example (Maekawa *et al.*, 1991). Such structural complexity, in turn, may affect other isotopic systems for which the isotopes interact with the Q^n units as reported, for example, for $^{15}N/^{14}N$ (Mysen and Fogel, 2010), for $^{13}C/^{12}C$ (Mysen *et al.*, 2009), or for the isotopes of S (Labidi *et al.*, 2016). Therefore, it might have played an important influence on the geochemical isotopic record used to reconstruct the history of the Earth and other silicate planets.

Acknowledgements

All NMR experiments were performed at the W.M. Keck Solid State NMR Facility at the Geophysical Laboratory, supported in part by the W.M. Keck Foundation. This research was supported in part by NSF grants EAR 121754 and EAR12504491, NASA Astrobiology and by the Carnegie Institution of Washington. The authors thank Jabrane Labidi and Anat Shahar (GL-CIW) for discussions on the present subject and their comments and corrections on the present manuscript, and Dionysis Foustoukos (GL-CIW) for helpful discussions and comments.

Editor: Bruce Watson

Additional Information

Supplementary Information accompanies this letter at www.geochemicalperspectivesletters.org/article1609

Reprints and permission information is available online at http://www.geochemicalperspectivesletters.org/copyright-and-permissions

Cite this letter as: Le Losq, C., Mysen, B.O., Cody, G.D. (2016) Intramolecular fractionation of hydrogen isotopes in silicate quenched melts. *Geochem. Persp. Let.* 2, 87-94.

References

Behrens, H., Yamashita, S. (2008) Water speciation in hydrous sodium tetrasilicate and hexasilicate melts: Constraint from high temperature NIR spectroscopy. *Chemical Geology* 256, 306-315.

Chacko, T., Cole, D.R., Horita, J. (2001) Equilibrium oxygen, hydrogen and carbon isotope fractionation factors applicable to geologic systems. *Reviews in mineralogy and geochemistry* 43, 1-81.

Dalou, C., Le Losq, C., Mysen, B.O. (2015) In situ study of the fractionation of hydrogen isotopes between aluminosilicate melts and coexisting aqueous fluids at high pressure and high temperature–Implications for the δD in magmatic processes. *Earth and Planetary Science Letters* 426, 158-166.

Dauphas, N., Roskosz, M., Alp, E.E., Neuville, D.R., Hu, M.Y., Sio, C.K., Cordier, C. (2014) Magma redox and structural controls on iron isotope variations in Earth's mantle and crust. *Earth and Planetary Science Letters* 398, 127-140.

De Hoog, J.C., Taylor, B.E., Van Bergen, M.J. (2009) Hydrogen-isotope systematics in degassing basaltic magma and application to Indonesian arc basalts. *Chemical Geology* 266, 256-266.

Driesner, T. (1997) The effect of pressure on deuterium-hydrogen fractionation in high-temperature water. *Science* 277, 791-794.

Gibbs, G.V., Ross, N.L., Cox, D.F., Rosso, K.M. (2014) Insights into the crystal chemistry of Earth materials rendered by electron density distributions: Pauling's rules revisited. *American Mineralogist* 99, 1071-1084.

Greaves, G.N., Sen, S. (2007) Inorganic glasses, glass-forming liquids and amorphizing solids. *Advances in Physics* 56, 1-166.

Horita, J., Driesner, T., Cole, D.R. (1999) Pressure effect on hydrogen isotope fractionation between brucite and water at elevated temperatures. *Science* 286, 1545-1547.

Horita, J., Cole, D.R., Polyakov, V.B., Driesner, T. (2002) Experimental and theoretical study of pressure effects on hydrogen isotope fractionation in the system brucite-water at elevated temperatures. *Geochimica et Cosmochimica Acta* 66, 3769-3788.

Horita, J., Dos Santos, A.M., Tulk, C.A., Chakoumakos, B.C., Polyakov, V.B. (2010) High-pressure neutron diffraction study on H–D isotope effects in brucite. *Physics and Chemistry of Minerals* 37, 741-749.

Labidi, J., Shahar, A., Le Losq, C., Hillgren, V.J., Mysen, B.O., Farquhar, J. (2016) Experimentally determined sulfur isotope fractionation between metal and silicate and implications for planetary differentiation. *Geochimica et Cosmochimica Acta* 175, 181-194.

Labrosse, S., Hernlund, J.W., Coltice, N. (2007) A crystallizing dense magma ocean at the base of the Earth's mantle. *Nature* 450, 866-869.

Le Losq, C., Mysen, B.O., Cody, G.D. (2015) Water and magmas: insights about the water solution mechanisms in alkali silicate melts from infrared, Raman, and ^{29}Si solid-state NMR spectroscopies. *Progress in Earth and Planetary Sciences* 2, 22, doi: 10.1186/s40645-015-0052-7.

Maekawa, H., Maekawa, T., Kawamura, K., Yokohama, T. (1991) The structural groups of alkali silicate glasses determined from ^{29}Si MAS-NMR. *Journal of Non-Crystalline Solids* 127, 53-64.

Mysen, B. (2013a) Hydrogen isotope fractionation between coexisting hydrous melt and silicate-saturated aqueous fluid: An experimental study in situ at high pressure and temperature. *American Mineralogist* 98, 376-386.

Mysen, B. (2013b) Effects of fluid and melt density and structure on high-pressure and high-temperature experimental studies of hydrogen isotope partitioning between coexisting melt and aqueous fluid. *American Mineralogist* 98, 1754-1764.

Mysen, B., Richet, P. (2005) Silicate glasses and melts: properties and structure. Vol. 10, Elsevier, Amsterdam, The Netherlands.

Mysen, B.O., Fogel, M.L. (2010) Nitrogen and hydrogen isotope compositions and solubility in silicate melts in equilibrium with reduced (N+H)-bearing fluids at high pressure and temperature: effects of melt structure. *American Mineralogist* 95, 987-999.

Mysen, B.O., Fogel, M.L., Morrill, P.L., Cody, G.D. (2009) Solution behavior of reduced C O H volatiles in silicate melts at high pressure and temperature. *Geochimica et Cosmochimica Acta* 73, 1696-1710.

Novak, A. (1974) Hydrogen bonding in solids correlation of spectroscopic and crystallographic data. In: *Large Molecules*. Springer Berlin Heidelberg, 177-216.

Robert, E., Whittington, A., Fayon, F., Pichavant, M., Massiot, D. (2001) Structural characterization of water-bearing silicate and aluminosilicate glasses by high-resolution solid-state NMR. *Chemical Geology* 174, 291-305.

Schauble, E.A. (2004) Applying stable isotope fractionation theory to new systems. *Reviews in Mineralogy and Geochemistry* 55, 65-111.

Wang, Y., Cody, S.X., Foustoukos, D., Mysen, B.O., Cody, G.D. (2015) Very large differences in intramolecular D-H partitioning in hydrated silicate melts synthesized at upper mantle pressures and temperatures. *American Mineralogist* 100, 1182-1189.

Wood, B.J., Walter, M.J., Wade, J. (2006) Accretion of the Earth and segregation of its core. *Nature* 441, 825-833.

Xue, X., Kanzaki, M. (2009) Proton distributions and hydrogen bonding in crystalline and glassy hydrous silicates and related inorganic materials: insights from high-resolution solid-state Nuclear Magnetic Resonance spectroscopy. *Journal of the American Ceramic Society* 92, 2803-2830.

Intramolecular fractionation of hydrogen isotopes in silicate quenched melts

C. Le Losq[1,2*], B.O. Mysen[1], G.D. Cody[1]

Supplementary Information

The Supplementary Information includes:

- Supplementary Methods and Results
- Table S-1
- Figures S-1 to S-4
- Supplementary Information References

Supplementary Methods and Results

Sample preparation

Anhydrous $Li_2Si_4O_9$ (LS4), $Na_2Si_4O_9$ (NS4) and $K_2Si_4O_9$ (KS4) glass starting materials used here are the same as those described in Le Losq *et al.* (2015a,b,c). Hydrous glasses, containing pure ^1H_2O, pure ^2H_2O or a 50:50 mixture of ^1H_2O-^2H_2O, were formed by temperature-quenching melts hydrated at high pressure and temperature in platinum capsules by using a piston-cylinder apparatus, following the protocol described in Le Losq *et al.* (2015a,b,c; see Table S-1 for water content measurements and experimental conditions).

Raman and NMR spectroscopy

Raman spectra were recorded with a Jasco® NRS 3100 spectrometer as described in Le Losq *et al.* (2015a,b). Raman spectra were recorded with a 2400 lines/mm grating, which results in an accuracy of ±3 cm^{-1}. Precision was ±1 cm^{-1}. Alignment

1. Geophysical Laboratory, Carnegie Institution of Washington, 5251 Broad Branch Road NW, 20015 Washington D.C., USA
2. Present address: Research School of Earth Sciences, The Australian National University, Building 142, Mills Road, ACT 2601 Canberra, Australia
* Corresponding author (email: charles.lelosq@anu.edu.au)

Table S-1 Water concentration and synthesis conditions of the quenched melts. Nom. water refers to the nominal ^1H_2O or ^2H_2O concentrations. *Endmembers* and *Mixed* respectively refer to the products containing only ^1H_2O or ^2H_2O, and to those prepared with the 50:50 mixture of ^2H_2O + ^1H_2O. ^1H_2O concentrations of *endmembers* are from Le Losq *et al.* (2015a,b). The Raman-based technique of Le Losq *et al.* (2015b) was used to determine the concentration of ^1H_2O, ^2H_2O or of ^1H_2O+^2H_2O in the glasses. However, as it has not been cross-validated with another technique for the ^2H_2O and ^1H_2O+^2H_2O concentrations, no error bars are provided. Other errors are given at the 1σ confidence interval.

Glass	nom. water, total mol%	Synthesis conditions	RAMAN		
			$[^1H_2O]$	$[^2H_2O]$	$^2H/^1H$
$Li_2Si_4O_9$	3.28 (*endmembers*)	1650 °C 1.5 GPa 90 min.	3.08(60)	4.25(-)	-
	9.40 (*endmembers*)		10.09(60)	10.60(-)	-
	9.40 (*mixed*)		10.10(-)		1.04(07)
	17.64 (*endmembers*)		18.74(60)	17.38(-)	-
$Na_2Si_4O_9$	3.28 (*endmembers*)	1450 °C 1.5 GPa 90 min.	3.44(67)	3.87(-)	-
	9.40 (*endmembers*)		9.46(67)	9.73(-)	-
	9.40 (*mixed*)		10.33(-)		1.00(02)
	17.64 (*endmembers*)		17.54(67)	17.02(-)	-
$K_2Si_4O_9$	3.28 (*endmembers*)	1550 °C 1.5 Gpa 90 min.	3.98(74)	3.68(-)	-
	9.40 (*endmembers*)		9.62(74)	8.14(-)	-
	9.40 (*mixed*)		8.07(-)		n.d.
	17.64 (*endmembers*)		15.95(74)	15.99(-)	-

of the Raman spectrometer was tested against the 520.7 cm^{-1} Raman peak of pure Si. All spectra reported in this study are unpolarised. They are not corrected from excitation line and temperature effects, as we are interested in observing changes at Raman shifts above ~400 cm^{-1}, where such correction is unnecessary (Neuville *et al.*, 2014).

For analysis of the signals assigned to vibrations of silicate units, Raman spectra were treated as follows. A simple horizontal constant baseline was adjusted to the intensity in the 1270-1300 cm^{-1} portion of spectra, where no signal is observed. After baseline removal, intensity was normalised to the total area of the spectra. Such a process allows quantitative comparison of spectra (*e.g.*, Le Losq *et al.*, 2012; Neuville *et al.*, 2014). For water content determination, the treatment of the Raman spectra is slightly different as the baseline is also fitted to the basis of the bands located near 2600 and 3600 cm^{-1}, respectively assigned to O-^{2}H and O-^{1}H stretching (see Foustoukos and Mysen, 2012, and references cited therein). It is described in detail in Le Losq *et al.* (2015b), such that we refer the reader to this publication.

Hydrogen-1 and Hydrogen-2 solid-state NMR experiments were carried out with a Varian-Chemagnetics CMX Infinity 300 solid-state NMR spectrometer with a static field strength of ~7.05 T. The ^{1}H spectra were acquired using a Magic Angle Spinning (MAS) frequency ($w_r/2\pi$) of 22 KHz, 16 cycle DEPTH sequence, ^{1}H pulse length of 2.5 µs, recycle delay of 100 s, and 1600 acquisitions. They are referenced to tetramethylsilane. See Cody *et al.* (2005) and Le Losq *et al.* (2015b) for further analytical details. Isotropic ^{2}H MAS NMR spectra, *i.e.* spectra that do not exhibit the classic effects of the ^{2}H quadrupolar coupling interaction, and that are therefore, completely comparable to the ^{1}H MAS NMR spectra, were obtained by rotor-synchronised acquisition following the protocol described in Wang *et al.* (2015).

Water concentrations

Water concentrations of the $^{1}H_2O$- and $^{2}H_2O$-bearing glasses were checked with Raman spectroscopy, using the calibration that links the glass water content measured by Infrared (or another technique) to the ratio between the areas of the Raman bands assigned to silicate vibrations and to the O-^{1}H or O-^{2}H stretching vibration as described by Le Losq *et al.* (2012). We used the calibration curve determined by Le Losq *et al.* (2015b) for simple alkali silicate glasses. The method has been shown to determine accurately the water content of natural glasses (Shea *et al.*, 2014; Métrich *et al.*, 2015).

The $^{2}H/^{1}H$ ratios were determined with the ratio of integrated areas of the Raman bands assigned to O-^{2}H and O-^{1}H stretch vibrations (Mysen, 2010; Foustoukos and Mysen, 2012; Dalou *et al.*, 2015). The method was validated with spectra of LS4 and NS4 glasses containing a nominal 50:50 mixture of $^{2}H_2O$ and $^{1}H_2O$. The area ratios of the Raman peaks assigned to the O-^{2}H and the O-^{1}H stretching vibrations lead to the nominal 50:50 $^{2}H/^{1}H$ ratio (Table S-1). For KS4 glasses, no $^{2}H/^{1}H$ ratio measurement was possible because the bands assigned to the O-^{1}H and O-^{2}H stretching vibrations overlap strongly. The fact that the $^{2}H/^{1}H$ ratios of the glasses as measured by the area ratio method agree with nominal values indicates that the Raman cross sections of the O-^{2}H and O-^{1}H stretching vibrations are similar at room temperature in glasses. As a consequence, the $^{1}H_2O$-based calibration of total water contents was used to estimate the $^{2}H_2O$ and the $^{1}H_2O$+$^{2}H_2O$ concentrations of the glasses. However, as it has not been cross-validated by another technique, no error bars are provided for those values (Table S-1).

Note on the interpretation of ^{1}H and ^{2}H MAS NMR spectra

The ^{1}H and ^{2}H isotropic MAS NMR spectra of all glasses exhibit two intense peaks located near 5 and 16 ppm with shoulders near 3.5 and 12 ppm, respectively, and a small sharp peak near 1.8 ppm (Figs. 1, S-1, S-2). These features

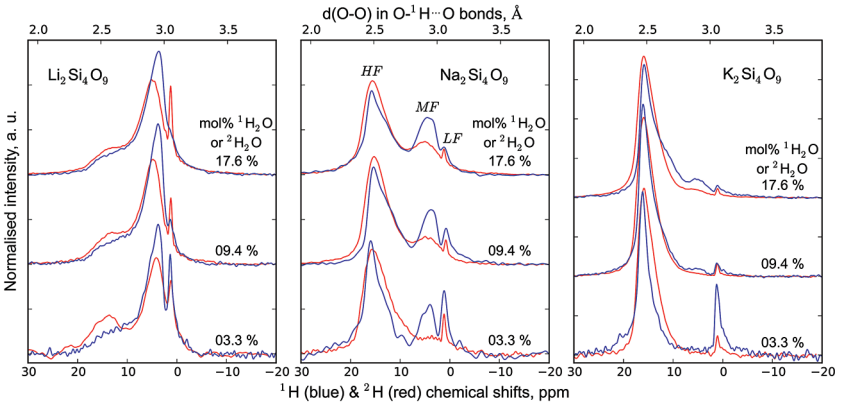

Figure S-1 Superposition of ^{1}H and ^{2}H isotropic MAS NMR spectra of the silicate glasses containing pure $^{1}H_2O$ or $^{2}H_2O$ for different $^{1}H_2O$ and $^{2}H_2O$ concentrations as indicated on individual spectra (mol %). Blue and red lines are the ^{1}H and ^{2}H NMR signals, respectively. The O-O distances of O-H···O bonds (with – an ionic-covalent bond and ··· a hydrogen bond) determined from the ^{1}H chemical shift (equation from Xue and Kanzaki, 2009) are shown on the upper horizontal axis.

correspond to protons and deuterons existing in, at least, 5 different environments in the silicate glasses (Le Losq *et al.*, 2015b and references therein).

The NMR spectra can be divided into three frequency regions (Figs. 1, S-1, S-2). The high (HF), middle (MF) and low (LF) frequency regions are centred on the main peaks near 16 ppm (encompassing the 12 ppm signal), 5 ppm (encompassing the 3.5 ppm signal) and 1.8ppm, respectively. These reflect ^{1}H nuclei in O-H···O environments with mean O-O distances of ~245, ~295 and 305 pm, respectively (Xue and Kanzaki, 2009 and references therein). The HF, MF and LF regions in the ^{2}H isotropic NMR spectra also correlate with the degree of shielding of ^{2}H, related to O-O distances (Wang *et al.*, 2015). Therefore, at constant water content, changes in the ^{1}H and ^{2}H isotropic NMR spectra reflect how both ^{1}H and ^{2}H populate environments with smaller O-O distances, and hence, smaller structural volumes with increasing ionic radius of the alkali metal (Figs. 1, S-1, S-2; Le Losq *et al.*, 2015b). At any given water content and alkali metal radius, differences between the isotropic ^{1}H and ^{2}H MAS NMR spectra are not due to instrumental or quench effects (Wang *et al.*, 2015) but reflect differences in the population of ^{1}H and ^{2}H nuclei between the different structural environments in the glasses.

The $\alpha_{HF\text{-}MF}$ (= $(^{2}H/^{1}H)_{HF}$ / $(^{2}H/^{1}H)_{MF}$) intramolecular fractionation factors have been obtained by first determining the $^{2}H_{HF}$, $^{1}H_{HF}$, $^{2}H_{MF}$ and $^{1}H_{MF}$ areas in the HF and LF regions of the ^{1}H and ^{2}H isotropic NMR spectra by trapezoidal integration, and then by dividing the integrated areas as ($^{2}H_{HF}/^{1}H_{HF}$) / ($^{2}H_{MF}/^{1}H_{MF}$).

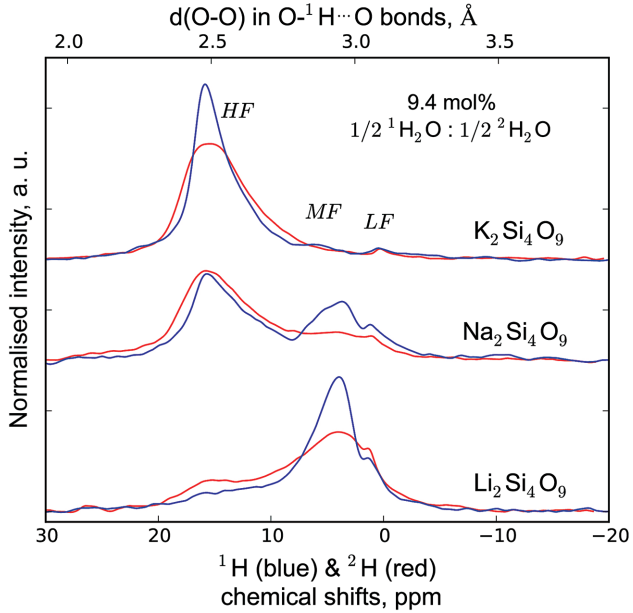

Figure S-2 ^{1}H and ^{2}H isotropic MAS NMR spectra of the alkali tetrasilicate glasses with ^1H_2O and ^2H_2O in a 1:1 molar ratio (total ^1H_2O + ^2H_2O molar content of 9.4 mol %). Blue lines and red lines are the ^{1}H and ^{2}H NMR signals, respectively. The O-O distances of O-H···O bonds determined from the ^{1}H chemical shift (equation from Xue and Kanzaki, 2009) are shown on the upper horizontal axis.

Assignment of bands and interpretation of Raman spectra of alkali silicate glasses

In alkali tetrasilicate melts at their glass transition temperature, water is dissolved as H_2O_{mol} molecules and as OH groups bonded to Si or the alkalis (Cody *et al.*, 2005; Mysen and Cody, 2005; Xue and Kanzaki, 2009; Le Losq *et al.*, 2015a). The distribution of the Q^n tetrahedral units (see Fig. 3) in hydrous silicate glasses changes as a function of the fraction of OH groups bonded to Si. This affects *in fine* the 850-1300 cm^{-1} portion of the glasses Raman spectra, in which peaks and shoulders can be assigned to Si-O stretching vibrations in specific Q^n units (Fig. 3a). In particular, signals at ~950, ~1040, ~1090, and ~1150 cm^{-1} are assigned to the symmetric stretching of Si-O bonds in Q^2 units, the asymmetric stretching of Si-O bonds in any Q^n units, and the symmetric stretching of Si-O bonds in Q^3 units and in Q^4 units, respectively (Brawer and White, 1975, 1977; Virgo *et al.*, 1980; Furukawa *et al.*, 1981; Mysen *et al.*, 1982; McMillan, 1984; see also peak fitting results in Mysen, 1990; Le Losq *et al.*, 2015a). Another signal near 900 cm^{-1} is visible in the Raman spectra of the hydrous alkali silicate glasses. This peak

is typically assigned to vibrations of OH groups bonded to the silicate network (McMillan *et al.*, 1993; Zotov and Keppler, 1998; Malfait, 2009; Spiekermann *et al.*, 2012). Note that its Raman shift decreases in frequency with substitution of ^{1}H by ^{2}H (Fig. 3a, S-3, S-4), indicating a role of ^{1}H and ^{2}H in the origin of this signal.

The prominent peak in all Raman spectra near 1100 cm^{-1}, assigned to Si-O stretching in Q^3 units, indicates that the latter units dominate in such glasses (Figs. 3a, S-3). Shoulders near 950 and 1150 cm^{-1}, assigned to the Si-O stretching in Q^2 and Q^4 units, indicate that small proportions of those silicate units are present in the quenched melts. This agrees with previous Raman and ^{29}Si NMR results (Mysen, 1990; Maekawa *et al.*, 1991; Zotov and Keppler, 1998; Mysen and Cody, 2005). With increasing water content in the glasses, the signals between 900-1100 cm^{-1} become more intense, reflecting the depolymerisation of the tetrahedral network that occurs with solution of water (Zotov and Keppler, 1998; Cody *et al.*, 2005; Mysen and Cody, 2005). Increasing the alkali ionic radius promotes the latter effect (Le Losq *et al.*, 2015a). Substitution of ^{1}H by ^{2}H results in increasing and decreasing the intensity of the signals assigned to Si-O stretching in Q^3 and Q^2 units, respectively (Figs. 3, S-3, S-4), reflecting the slight preferential bonding of ^{2}H to Q^3 units.

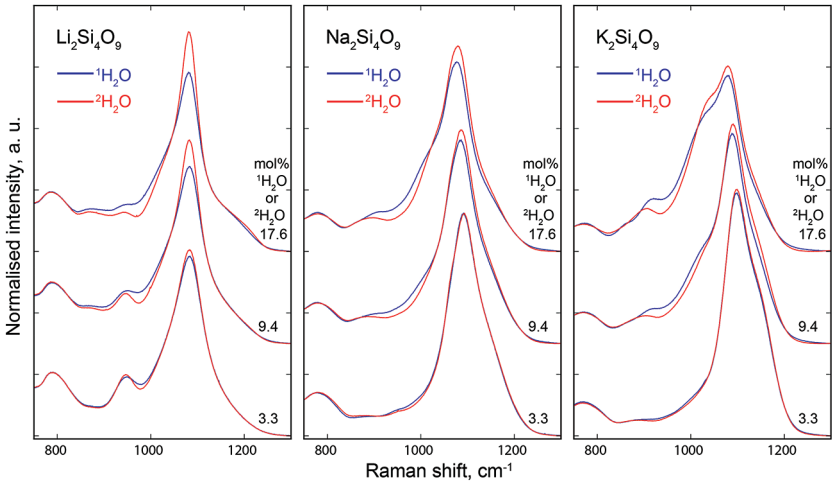

Figure S-3 750-1300 cm^{-1} portion of all the Raman spectra of the alkali silicate glasses containing pure ^1H_2O (blue lines) or ^2H_2O (red lines). ^1H_2O / ^2H_2O mol % concentrations are indicated at the right end of each spectrum. See text for discussion and attributions.

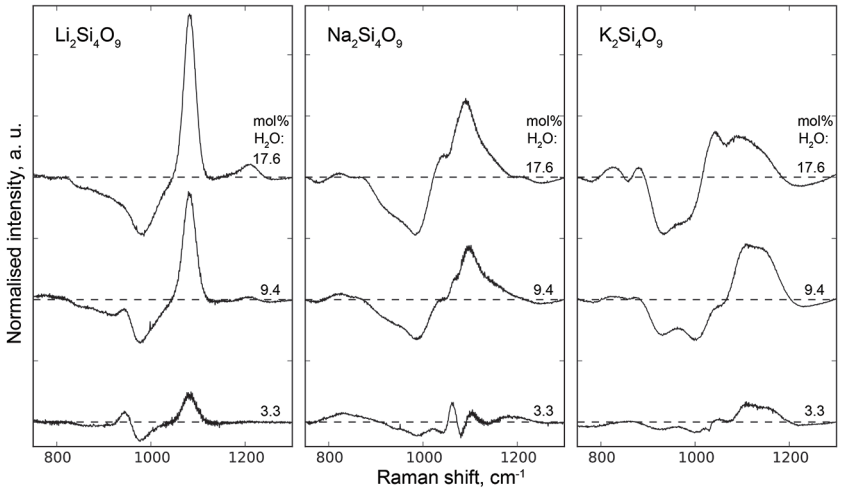

Figure S-4 Residual Raman signals after subtraction of the Raman spectra of ^1H_2O-bearing glasses from those of ^2H_2O-bearing glasses. Dashed horizontal lines indicate the 0 value for each residual spectrum. Water concentrations, as mol % ^1H_2O or ^2H_2O, are indicated at the right end of each residual signal. Positive peaks indicate increasing intensity with substitution of ^1H by ^2H, and negative peaks the opposite case. Systematic increase of intensity near 1100 cm^{-1} is observed, while intensity systematically decreases near 950-1000 cm^{-1}. Those changes reflect increasing and decreasing contributions of Q^3 and Q^2 units to the Raman signal, respectively, with substitution of ^1H by ^2H. The contributions between 850 and 930 cm^{-1} are artifacts resulting from the frequency shift of the Si-O-H stretching vibration upon $^2H/^1H$ substitution.

Supplementary Information References

Brawer, S.A., White, W.B. (1975) Raman spectroscopic investigation of the structure of silicate glasses. I. The binary alkali silicates. *The Journal of Chemical Physics* 63, 2421-2432.

Brawer, S.A., White, W.B. (1977) Raman spectroscopic investigation of the structure of silicate glasses (II). Soda-Alkaline earth-Alumina ternary and quaternary glasses. *Journal of Non-Crystalline Solids* 23, 261-278.

Cody, G.D., Mysen, B.O., Lee, S.K. (2005) Structure vs. composition: A solid-state ^1H and ^{29}Si NMR study of quenched glasses along the Na_2O-SiO_2-H_2O join. *Geochimica et Cosmochimica Acta* 69, 2373-2384.

Dalou, C., Le Losq, C., Mysen, B.O. (2015) In situ study of the fractionation of hydrogen isotopes between aluminosilicate melts and coexisting aqueous fluids at high pressure and high temperature–Implications for the δD in magmatic processes. *Earth and Planetary Science Letters* 426, 158-166.

Foustoukos, D.I., Mysen, B.O. (2012) D/H fractionation in the H_2–H_2O system at supercritical water conditions: compositional and hydrogen bonding effects. *Geochimica et Cosmochimica Acta* 86, 88-102.

Furukawa, T., Fox, K.E., White, W.B. (1981) Raman spectroscopic investigation of the structure of silicate glasses. III. Raman intensities and structural units in sodium silicate glasses. *Journal of Chemical Physics* 75, 3226-3237.

Le Losq, C., Neuville, D.R., Moretti, R., Roux, J. (2012) Determination of Water Content in Silicate Glasses using Raman Spectrometry, Implications for the study of explosive volcanism. *American Mineralogist 97*, 779-790.

Le Losq, C., Mysen, B.O., Cody, G.D. (2015a) Water and magmas: insights about the water solution mechanisms in alkali silicate melts from infrared, Raman, and ^{29}Si solid-state NMR spectroscopies. *Progress in Earth and Planetary Sciences* 2, 22, doi: 10.1186/s40645-015-0052-7.

Le Losq, C., Cody, G.D., Mysen, B.O. (2015b) Alkali influence on the water speciation and the environment of protons in silicate glasses revealed by ^1H MAS NMR spectroscopy. *American Mineralogist* 100, 466-473.

Le Losq, C., Cody, G.D., Mysen, B.O. (2015c) Complex stretching signal of OH groups in silicate glasses: implication for the use of the 4500 cm^{-1} IR peak as a marker of OH^- groups concentration. *American Mineralogist* 100, 945-950.

Maekawa, H., Maekawa, T., Kawamura, K., Yokohama, T. (1991) The structural groups of alkali silicate glasses determined from ^{29}Si MAS-NMR. *Journal of Non-Crystalline Solids* 127, 53-64.

Malfait, W.J. (2009) The 4500 cm^{-1} infrared absorption band in hydrous aluminosilicate glasses is a combination band of the fundamental {Si,Al}-OH and O-H vibrations. *American Mineralogist* 94, 849-852.

McMillan, P.F. (1984) Structural studies of silicate glasses and melts - Applications and limitations of Raman spectroscopy. *American Mineralogist* 69, 622-644.

McMillan, P.F., Poe, B.T., Stanton, T.R., Remmele, R.L. (1993) A Raman spectroscopic study of H/D isotopically substituted hydrous aluminosilicate glasses. *Physic and Chemistry of Minerals* 19, 454-459.

Métrich, N., Bertagnini, A., Garaebiti, E., Vergniolle, S., Bani, P., Beaumais, A., Neuville, D.R. (2015) Magma transfer and degassing budget: Application to the 2009–2010 eruptive crisis of Mt Garet (Vanuatu arc). *Journal of Volcanology and Geothermal Research*, doi:10.1016/j.jvolgeores.2015.06.003.

Mysen, B.O. (1990) Role of Al in depolymerized, peralkaline aluminosilicate melts in the systems Li_2O-Al_2O_3-SiO_2, Na_2O-Al_2O_3-SiO_2, and K_2O-Al_2O_3-SiO_2. *American Mineralogist* 75, 120-134.

Mysen, B.O., Fogel, M.L. (2010) Nitrogen and hydrogen isotope compositions and solubility in silicate melts in equilibrium with reduced (N+H)-bearing fluids at high pressure and temperature: effects of melt structure. *American Mineralogist* 95, 987-999.

Mysen, B.O., Cody, G. (2005) Solution mechanisms of H_2O in depolymerized peralkaline melts. *Geochimica et Cosmochimica Acta* 69, 5557-5566.

Mysen, B.O., Finger, L.W., Virgo, D., Seifert, F.A. (1982) Curve-fitting of Raman spectra of silicate glasses. *American Mineralogist* 67, 686-695.

Neuville, D.R., de Ligny, D., Henderson, G.S. (2014) Advances in Raman spectroscopy applied to earth and material sciences. *Reviews in Mineralogy and Geochemistry 78*, 509-541.

Shea, T., Hellebrand, E., Gurioli, L., Tuffen, H. (2014) Conduit-to localized-scale degassing during Plinian Eruptions: Insights from major element and volatile (Cl and H_2O) analyses within Vesuvius AD 79 pumice. *Journal of Petrology* 55, 315-344.

Spiekermann, G., Steel-McInnis, M., Schmidt, C., Jahn, S. (2012) Vibrational mode frequencies of silica species in SiO_2-H_2O liquids and glasses from ab initio molecular dynamics. *The Journal of Chemical Physics* 136, 154501.

Virgo, D., Mysen, B.O., Kushiro, I. (1980) Anionic constitution of silicate melts quenched at 1 atm from Raman spectroscopy: Implications for the structure of igneous melts. *Science* 208, 1371-1373.

Wang, Y., Cody, S.X., Foustoukos, D., Mysen, B.O., Cody, G.D. (2015) Very large differences in intramolecular D-H partitioning in hydrated silicate melts synthesized at upper mantle pressures and temperatures. *American Mineralogist* 100, 1182-1189.

XUE, X., KANZAKI, M. (2009) Proton distributions and hydrogen bonding in crystalline and glassy hydrous silicates and related inorganic materials: insights from high-resolution solid-state Nuclear Magnetic Resonance spectroscopy. *Journal of the American Ceramic Society* 92, 2803-2830.

ZOTOV, N., KEPPLER, H. (1998) The influence of water on the structure of hydrous sodium tetrasilicate glasses. *American Mineralogist* 83, 823-834.